Immobilization of lead from aqueous solution by using carboxymethyl cellulose stabilized iron sulfide nanoparticles

by

Yang Zhao

A thesis submitted to the Graduate Faculty of
Auburn University
in partial fulfillment of the
requirements for the Degree of
Master of Science

Auburn, Alabama
December 16, 2017

Keywords: Nanomaterials; Nanoparticles; Iron sulfide; Lead; Carboxymethyl cellulose; CMC; Stabilized nanoparticles; Precipitation; Surface complexation

Approved by

Dongye Zhao, Chair, Elton Z. and Lois G. Huff Professor of Civil/Environmental Engineering
Mark O. Barnett, Malcolm Pirnie Professor of Civil Engineering
Clifford R. Lange, Associate Professor of Civil Engineering

Abstract

Lead pollutant has attracted more attention recently. Moreover, the use of patent iron sulfide nanoparticles is more and more extensive for various contaminants removal. In this study, FeS nanoparticles is prepared with carboxymethyl cellulose (CMC) as a stabilizer, which can be used for improving removal of aqueous lead (Pb^{2+}). Firstly, to find the specific mechanism during the removal, batch tests such as kinetic with curve fitting, isotherm with model fitting, FTIR spectra and XRD have been done. In these experiments, the pseudo-second-order kinetic curve fitting indicates that the reaction is rapid in the beginning, and the rate-controlling step for adsorption is chemical interaction. The isotherm curve shows S-shape with Sigmoidal isotherm model fitting, which means at low Pb^{2+} concentration the complexation between Pb and CMC phase competes with the Pb sorption, and the main adsorption mechanism is surface complexation. FTIR and XRD analyses indicate the same results that precipitation (formation of Galena PbS) and surface complexation are important mechanisms for lead removal. Secondly, for obtaining the optimal removal conditions, FeS dosage test, CMC-to-FeS molar ratio test, DLS size and zeta potential test and effect test of pH, coexisting ions and leonardite HA have been done. The best FeS dosage and CMC-FeS molar ratio are 50 mg/L FeS and 0.0005 (50 mg/L FeS: 0.0025 wt % CMC). When the CMC-to-FeS molar ratio $\geq$ 0.0005, the particles are fully stabilized. High lead uptake is observed over the pH range of 6.5~7.0, whereas significant capacity loss is observed at pH < 6 since the large amount of FeS particle leaching in the acid environment. And the result of DLS size and zeta potential test demonstrate that the CMC-FeS particles are nanoscale with larger specific surface area, and the zeta potential is negative for effective Pb^{2+} adsorption. High concentrations of Na^{+} and Ca^{2+} ($\geq$ 10 mM) and leonardite HA

(10 mg/L as TOC) modestly inhibit the lead uptake. Thus, the experimental results verify that the proposed CMC-FeS nanoparticles can remove Pb^{2+} efficiently with the main mechanisms of precipitation and surface complexation.

Acknowledgments

First, I would like to appreciate my advisor, Dr. Dongye Zhao, who has supported me throughout my research and thesis with his guidance, patience, motivation and knowledge. During the research he not only taught me the knowledge, but also encourage me to be a hardworking and wise researcher. Without his help and support, I would never have been able to finish my thesis.

Besides, I'd like to thank my thesis committees: Dr. Mark O. Barnett, and Dr. Clifford R. Lange for their insightful comments. Especially, I am grateful to Dr. Mark O. Barnett, who recommended me to be a teaching assistant in Chemistry Department. The experience helps me to improve my oral communication and consolidate experiment operations.

During the research period, I thank Dr. Byron H. Farnum and his graduate student Alexandria Combs in Chemistry and Biochemistry Department in Auburn University for their machine support and assistance with the FTIR machine operation and result analysis. I also thank Mr. Steven Moore in Materials Engineering in Auburn University for his help with the XRD machine operation.

I am so glad to be a member of our friendly and sweet research group. I would like to thank Shuting Tian and Wen Liu for their teaching me the basic experiment skills in our lab. And I'd especially like to thank Yanyan Gong for her help with my manuscript revision.

Finally, I'd like to express my love and gratitude to my husband, Xuyu Wang, for his encouragement and help with my thesis revision. Thank my parents for supporting me spiritually and financially throughout my life.

Table of Contents

List of Tables

List of Figures

List of Abbreviations

CMC	Carboxymethyl cellulose
FTIR	Fourier-transform infrared spectroscopy
XRD	X-ray Diffraction
DLS	Dynamic light scattering
HA	Humic Acid
DI Water	Deionized water
DO	Dissolved oxygen
ICDD	International Centre for Diffraction Data
CSC	Critical stabilization concentration
TOC	Total organic carbon
DOM	Dissolved organic matter

Chapter 1

Introduction

1.1 Background

1.1.1 Lead Pollution Sources

With the rapid development of industrial production, lead is widely used, which has been a significant metal in human societies for thousands of years. Lead (Pb) is one of the most common hazardous heavy metals in water due to increasing human activities such as lead mining, lead smelting, battery manufacturing, and e-waste recycling. The poisoning is usually caused by ingestion of lead contaminated food and water, and less occurs after accidental ingestion of contaminated soil, dust or lead-based paints [1]. Once seawater products are contaminated by nearby industrial water, they will contain lead [2]. Fruits and vegetables may be affected by high levels of lead in the soil which may be contaminated by lead in the pipeline, lead paint and residual emissions from lead gasoline [3]. In our daily life, lead pollution is mainly from e-waste recycle [4], urban dust [5] [6], industry wastes (e.g. chemical, coking, mining and glass) [7] [8], and so on. For urban dust, the sources are mainly from street dust, which mainly includes materials worn off the pavement, vehicular-related deposition particles (vehicle exhaust particles, lubricating oil residues, tire wear particles, brake lining wear particles) [5], and roof dust [9]. They are mainly from the atmospheric deposition. These pollutants will be dissolved by the rain, flow to the ground, and form the groundwater pollution [10], which harms to crops, livestock, humans and the ecosystem. It should be treated if the contaminant concentration of the groundwater is exceeded the maximum contaminant level (MCL) in drinking water of 0.015 mg/L Pb in the US National Drinking Water Standards (US

Environmental Protection Agency, May 2009). And the related companies need to consider whether the emissions meet the standard before discharge. Usually, except for occupational exposure we almost have no chance to contact high concentration of Pb contaminant directly in our daily life. From the Pb contaminant origin mentioned above, almost the wastewater contains low level concentration of Pb, which needs to be treated. And the normal range for pH in surface water systems is 6.5 to 8.5, and for groundwater systems is 6 to 8.5 [36]. And based on the low K_{sp} value of $Pb(OH)_2$ (1.43×10^{-20} at 25 °C), the solubility of Pb is about 294 ppb at pH 7.0 and 2.94 ppb at pH 8.0 in aqueous phase. Therefore, it becomes more important to remove wastewater with low Pb concentration in aqueous phase.

1.1.2 Lead Toxicology

Lead is a highly poisonous metal (whether inhaled or swallowed), where main ingested lead is obtained into bloodstream [40].The reason for its toxicity is the predilection for influencing the main function of enzymes, which is implemented by mimicking and displacing other metals acting as cofactors in several enzymatic reactions [42] or binding to the sulfhydryl groups on some enzymes [41]. The blood lead level above 25 μg/dl will harm to human health [43]. For high levels of human exposure, almost there is damage to all organs and organ systems, especially the central nervous system, kidneys and blood, culminating in death at excessive levels. For low levels, heme synthesis and other biochemical processes are affected. Psychological and neurobehavioral functions are also affected, as well as a range of other effects [43]. The potential negative effect of lead exposure is larger than adults. The main reasons are following. First, children intake of lead per unit body weight, which is larger than adults. Second, because young children often put objects into mouths, dust and soil are greatly ingested, leading

to increasing the intake of lead. Third, physiological uptake rates of lead for children are higher than for adults; Fourth, young children systems are not completely developed, and thus they are more vulnerable than adults for the intake of lead [44][45]. Moreover, the accumulated epidemiological evidence shows that such exposure in young children leads to a great deficit in cognitive development during the immediately ensuing childhood years [46], which is largely irreversible [47].

1.1.3 Lead Removal Methods

To mitigate human exposure to Pb, various technologies have been investigated for Pb removal from aqueous solutions, including chemical precipitation, ion exchange, adsorption, membrane filtration, coagulation-flocculation, flotation, electrochemical techniques [11], phytoremediation and microremediation [12] and bio-sorbents [11][13]. However, chemical precipitation is only effective for the treatment of wastewater with high concentrations of heavy metals. It is highly cost and can produce sludge in large quantities. Ion exchange, can handle wastewater with low concentrations of heavy metals, however, the process is expensive and causes serious secondary pollution during regeneration process. Similarly, membrane filtration, coagulation-flocculation, flotation, electrochemical methods are costly, and the processes are very complex. Thus, it is quiet challenging to meet the MCL of 15 µg/L of Pb in a cost-effective way.

Adsorption is a widely accepted method for the removal of aqueous heavy metals with low concentration [11]. Naturally occurring sulfide minerals mackinawite (FeS) and synthetic bulk FeS materials have been reported to be highly efficient immobilization agents for heavy metals, namely, Hg, Cu, Cr, and Pb [14], due to their unique molecular structure and surface chemical properties [14]. Bacterially-produced magnetic FeS can immobilize Pb through magnetic

adsorption [18]. It is reported that 1000 mg/L FeS can immobilize 98% Pb from initial 10 ppm to final 200 ppb in aqueous [18].

Nanoscale FeS materials are expected to offer better stability and higher immobilization capacity compared with bare FeS particles due to their larger specific surface area, potentially more active sorption sites, and high surface reactivity. Our previous researches proved that carboxymethyl cellulose (CMC), a polysaccharide stabilizer, effectively stabilized the FeS particles through concurrent steric hindrance and electrostatic repulsion, forming FeS nanoparticles (CMC-FeS) with an average particle size of 34 nm [15][16]. The resultant nanoparticles effectively immobilized aqueous Hg via chemical precipitation, ion exchange, and surface complexation with a much greater maximum sorption capacity of 3449 mg/g than other reported FeS [22][37]. However, to our best knowledge, the comprehensive investigations of CMC-FeS nanoparticles applied as adsorbents to immobilize Pb in aqueous solutions under various environmental conditions have not yet been explored [17][18][19].

1.2 Objectives

The overall goal of this study is to explore the performance of CMC-FeS in Pb immobilization from aqueous solutions. The specific objectives are to: (1) prepare various FeS particles with different CMC-to-FeS molar ratios and compare their Pb immobilization effectiveness; (2) examine effects of operation conditions including reaction time, FeS dosage, initial Pb concentrations, pH, coexisting ions, and leonardite humic acid (HA) on Pb removal by CMC-FeS nanoparticles in details; and (3) elucidate the underlying immobilization mechanisms.

1.3 Organization

In this article, the organization follows a standard thesis based on the Electronic Thesis and Dissertation Guide by the Auburn University Graduate School. Chapter 1 presents the introduction of the article. Chapter 2 states the materials and methods of this research. And chapter 3 shows the research results and discussion part. Above all, the chapter 4 gives the conclusion and recommendation for the future work.

Chapter 2

Materials and Methods

2.1 Chemicals

All chemicals used in this study were in the analytical grade or higher. Iron sulfate heptahydrate ($FeSO_4 \cdot 7H_2O$), carboxymethyl cellulose (CMC, in sodium form, molecular weight = 90,000, degree of substitute = 0.7), and humic acid (HA) (leonardite HA) were obtained from Acros Organics (Morris Plains, NJ, USA). Sodium sulfide nonahydrate ($Na_2S \cdot 9H_2O$), lead chloride ($PbCl_2$, F.W. = 278.12, CAS No. 7758-95-4), sodium hydroxide (NaOH), sodium nitrate (NaCl), and calcium nitrate ($CaCl_2$) were purchased from Fisher Scientific (Fair Lawn, NJ, USA). During the experiments, the deionized water (DI water, 18 MΩ cm) was used for all solutions preparation. Pb^{2+} stock solution (1000 mg/L) was prepared by dissolving 1.3423g $PbCl_2$ powder in DI water by using magnetic stirrer under low-temperature heating (50 ºC). And Pb^{2+} working solutions of 5 mg/L and 200 mg/L were diluted by mixing 5 mL and 200 mL of Pb^{2+} stock solution with 995 mL and 800 mL DI water, respectively.

2.2 Preparation and characterization of CMC-FeS nanoparticles

CMC-FeS nanoparticles were synthesized based on the reaction of Na_2S with $FeSO_4$ in the presence of CMC [20], and 200 mL nanoparticles CMC-FeS were prepared as the procedures in detail shown as below. In brief, under continuous N_2 purging, 1 mL CMC (1%, w/w), 169 mL DI water, and 20 mL $FeSO_4$ (11.4 mM) were added into 250 mL flask to yield a solution with desired concentrations of Fe^{2+} and CMC. Stoichiometric amounts of Na_2S solution (22.8 mM in

N_2-purged DI water) were added dropwise into the mixture under shaking at 150 rpm and vacuum to produce FeS nanoparticles. The resultant suspensions containing 100 mg/L FeS and 0.005 wt % CMC (i.e., a CMC-to-FeS molar ratio of 0.0005) were sealed under anaerobic conditions and aged for 24 h to ensure the full growth of CMC-FeS nanoparticles. FeS particles with various CMC-to-FeS molar ratios of 0, 0.0001, 0.0002, 0.0004, 0.0008, 0.0010, 0.0015, 0.0020 and 0.0025 were prepared following the same procedure except CMC stabilizer was applied at different amounts.

2.3 Effects of CMC concentration on stability of FeS nanoparticles and lead sorption capacity

To test the effects of CMC, FeS particles were prepared at a fixed FeS concentration of 50 mg/L as FeS but with various concentrations of CMC, namely, CMC-to-FeS molar ratios of 0, 0.0001, 0.0002, 0.0004, 0.0005, 0.0008, 0.0010, 0.0015, 0.0020 and 0.0025. The prepared particles were aged for 24 hours before use. After aged, different CMC-FeS molar ratio particles reacted with same initial conc. of Pb^{2+} (250 ppb) at initial pH 7, respectively. The particle stability was compared by measuring particle concentrations in the supernatants, which was determined by dissolving the FeS particles with 3M HNO_3. Fe concentration was measured using ICP-OES 710 ES (Agilent Technologies, Santa Clara, CA, USA). The detection limit of Pb is 5 ppb discussed in Appendices. The Pb^{2+} sorption capacities of the particles were conducted in the same way as in the isotherm tests.

2.4 Sorption kinetics

Batch kinetic tests were carried out in 20 mL sealed glass bottles under anaerobic conditions. The initial CMC-FeS and Pb concentrations were set at 50 mg/L FeS (CMC-to-FeS molar ratio of 0.0005) and 250 ppb, respectively. The total volume of each reaction solution was 200 mL containing 50 mg/L FeS and 0.0025 wt % CMC (CMC-to-FeS molar ratio of 0.0005) and 250 ppb initial concentration Pb^{2+} at pH 7.0±0.2. The pH was kept constant at pH 7.0±0.2 with HCl (1M, 0.1M) and/or NaOH (1M, 0.1M). The mixtures were continuously mixed on an end-over-end rotator at 30 rpm at room temperature (20±2 °C). At predetermined time intervals (5 min, 20 min, 40 min, 60 min (1 h), 90 min (1.5 h), 120 min (2 h), 240 min (4 h), 480 min (8 h), 720 min (12 h), 1440 min (24 h) (10 points)), duplicate sample were sacrificially sampled. The samples were filtered through a 25 nm membrane filter of nitrocellulose (Millipore Corp., Billerica, MA, USA), acidified with 0.05 mL 1 M HNO_3, and then analyzed for Pb using a ICP-OES 710-ES. Control tests were carried out in the absence of CMC-FeS under otherwise identical conditions. For comparison, sorption kinetic tests were also performed with non-stabilized FeS particles.

2.5 Lead sorption isotherm tests

Lead sorption isotherms with CMC-FeS were operated by carrying out equilibrium experiments in 30 mL glass bottles in duplicate. The experimental conditions were: FeS (a CMC-to-FeS molar ratio of 0.0005) = 25 mg/L, total added Pb^{2+} = 500 to 7000 ppb. It is noteworthy that the maximum solubility of lead at pH 7.0 was 294 ppb (K_{sp} value of $Pb(OH)_2$ = 1.43×10^{-20}). Therefore, to avoid the formation of $Pb(OH)_2$ precipitation, Pb^{2+} solution was intermittently added to the reaction system to achieve various concentrations. 38 µL of 200 mg/L Pb^{2+} solution was first added to the 30 mL nanoparticles. Upon equilibrium, another 38 µL Pb^{2+} solution was

added, resulting in an initial Pb^{2+} concentration of 500 ppb. The total added Pb^{2+} concentrations of 500, 1000, 1500, 2000, 2500, 3000, 4000, 5000, 6000, 7000 µg/L were obtained by continuously repeating the abovementioned procedure. The vials were equilibrated for 24 h in the same manner as in the kinetic tests.

2.6 Effects of CMC-FeS dosage, pH, humic acid, and Coexisting ions

Batch equilibrium sorption experiments were conducted in 30 mL vials to explore the effects of CMC-FeS dosage, reaction pH, leonardite HA, and coexisting cations on Pb^{2+} immobilization. To test the effect of CMC-FeS dosage, different concentrations of CMC-FeS (10, 25, 50, 75, 100, and 125 mg/L) with the same CMC-to- FeS molar ratio of 0.0005 were mixed with 250 ppb of Pb^{2+} at a fixed pH of 7. To investigate pH effect, batch equilibrium sorption tests were operated with 50 mg/L of CMC-FeS and 250 ppb of Pb^{2+} at initial pH values of 4.0, 4.5, 5.0, 5.5, 6.0, 6.5 and 7.0, and the final pH was provided in respective figure captions. To explore the HA effect, various concentrations of HA (1, 2, 5 and 10 ppm as TOC) were obtained by adding different amounts of HA solution (100 mg/L as TOC) into the mixture. To examine the coexisting ions effect, various concentrations of Na^{+} (0, 1, 2, 5 and 10 mM) and Ca^{2+} (0, 1, 2, 5 and 10 mM) were achieved with the addition of different volumes of NaCl solution (0.1 M) and $CaCl_2$ (0.1 M) into the suspensions, respectively. Control tests without the addition of CMC-FeS nanoparticles were conducted under otherwise identical conditions.

2.7 Viscosity, Particle size and Zeta potential

The hydrodynamic diameter and zeta potential were analyzed using a Malvern Zetasizer Nano ZS (Malvern Instruments, Worcestershire, U.K.). It should be noted that for the non-stabilized FeS particles, sonication was performed before analysis to break the aggregates. The resultant values were corrected with the viscosity of FeS particles with various concentrations of CMC, which was measured using a Gilmont falling ball viscometer (Thermo Fisher Scientific, Waltham, Massachusetts, USA). The size #1 Glass Falling Ball (range in cp. 0.2~2) was used in the viscosity measurement. We recorded the time and calculated the viscosity μ (cp) by the equation:

$$\mu = K(\rho_f - \rho)t$$

where K for Size #1 is 0.3, ρ_f for glass falling ball is 2.53, ρ is the liquid density, t is the time with minute.

2.8 XRD and FTIR test

The chemical compositions and crystallographic structure of the CMC-FeS nanoparticles before and after lead sorption as well as the sorbed Pb were performed by X-ray Diffractometer (XRD) using a Bruker D8 Discover X-Ray Diffractometer (Bruker Corporation, Billerica, Massachusetts, USA). The CMC-FeS nanoparticles before Pb immobilization were prepared at 500 mg/L as FeS with a CMC-to-FeS molar ratio of 0.0005 in 500 mL suspension. The nanoparticles after lead sorption were prepared with 500 mg/L of CMC-FeS (CMC-to-FeS molar ratio of 0.0005) and 20 mg/L Pb^{2+} in 500 mL suspension following the procedure as described in Section 2.4 with an equilibration time of 24 hours. For XRD analysis, the samples were collected by filtering the suspensions using a 25 nm nitrocellulose membrane filter. The solids were then

rinsed three times with N_2-purged DI water, and subsequently dried at 50 ºC (change the others accordingly) under N_2 protection for 72 hours using a Precision Economy Incubator (Precision, Winchester, VA, USA). The samples were grinded to powder and sealed for further analysis. For comparison, non-stabilized FeS particles were prepared without the CMC stabilizer but under otherwise identical conditions. The samples were placed in a zero background sample holder and scanned from 10° to 80° 2θ angles using a step interval of 0.01°, a step time of 0.1 s, and a scan speed of 6°/min. The resultant spectra were processed using MDI Jade 6.5 loaded with ICDD database (Materials Dara Inc., Livermore, CA, U.S.A.).

Fourier transform infrared (FTIR) spectroscopy measurements were conducted to explore interactions between CMC and FeS, and between lead and CMC-FeS. The dried samples were measured using a Thermo Scientific Nicolet iS50 FT-IR Spectrometer (Thermo Fisher Scientific, Waltham, Massachusetts, USA). For comparison, FTIR spectra for neat CMC and non-stabilized FeS particles was also acquired in the same manner.

Chapter 3

Results and Discussion

3.1 Lead Sorption Kinetics.

Adsorption kinetics of Pb(II) by non-stabilized FeS and CMC-FeS nanoparticles are compared in Figure 1(a). Control tests indicate that no lead is removed during the process. The lead concentration profile shows a rapid initial decrease during the early 2 hours (especially the initial 30 mins) followed by a slow drop stage until equilibrium at 40 minutes, which is consistent with the common notion that more active sites are taken up first. Upon equilibrium, the aqueous Pb concentration is 5 ppb, which meets the MCL of 15 µg/L of Pb.

The commonly used pseudo-first-order and pseudo-second-order kinetic models are utilized to analyze the sorption kinetic data [21]:

Pseudo-first-order kinetic model: $q_t = q_e - q_e \exp(-k_1 t)$

Pseudo-second-order kinetic model: $\frac{t}{q_t} = \frac{1}{k_2 q_e^2} + \frac{t}{q_e}$

in which k_1 (min-1) and k_2 (g mg^{-1} min^{-1}) are the rate constants of the pseudo-first-order and pseudo-second-order kinetic models, respectively. q_t and q_e (mg g^{-1}) are the adsorption capacities of lead at time t (min) and equilibrium time, respectively. The fitting results are shown in Figure 1(b) and the resultant fitting parameters are summarized in Table 1.

The kinetic results are closely fitted by the pseudo-second-order model, with a high correlation coefficient (R^2 = 0.9996). This illustrates that the rate-controlling step for adsorption is chemical interaction, which exhibits by the initial diffusion of metal ions from solution to CMC-FeS surface.

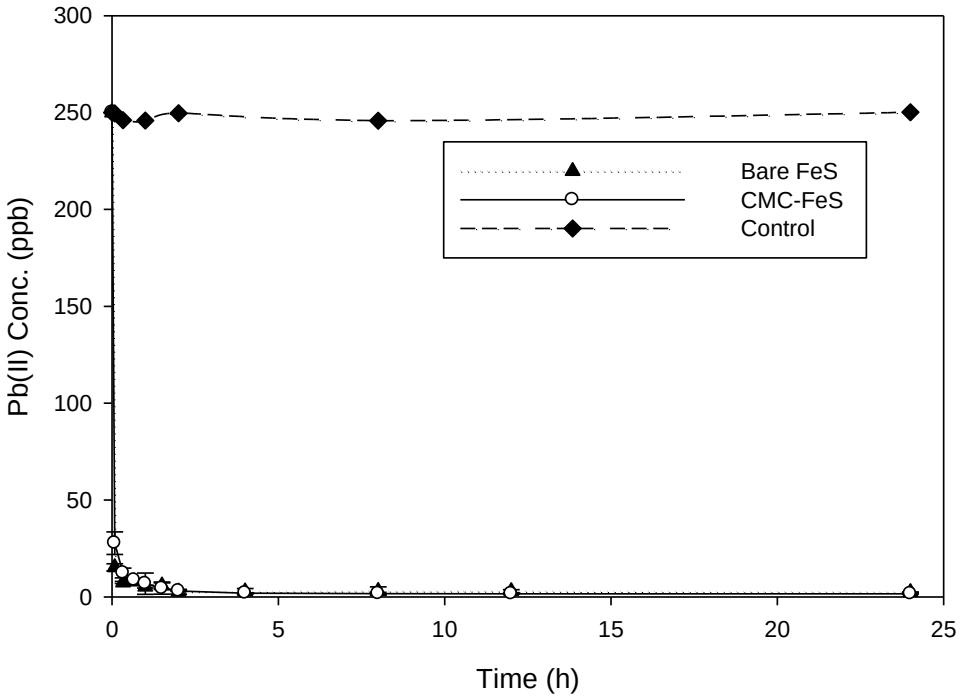

Figure 1(a). Lead sorption kinetics by CMC-FeS, bare FeS and Control. Initial Pb^{2+} = 250 ppb, FeS =50 mg/L, CMC-to-FeS molar ratio = 0.0005, pH =7.0±0.2. Data plotted as mean of duplicates and the error bars (calculated as standard deviation) indicate date reproducibility.

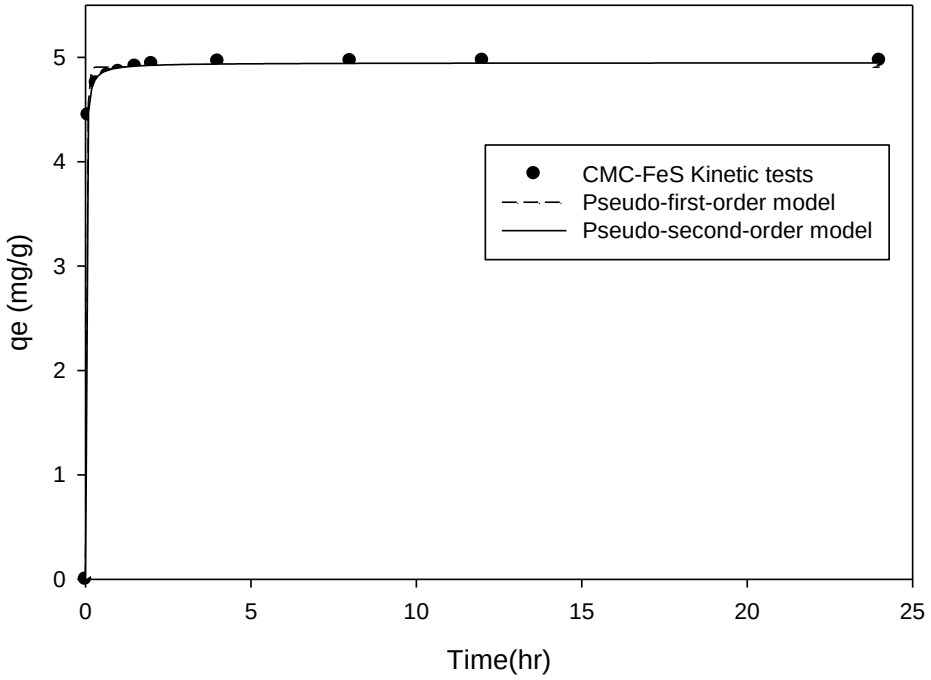

Figure 1(b). Pseudo-first-order and Pseudo-second-order kinetic fittings of lead sorption by CMC-FeS. Initial Pb^{2+} = 250 ppb, FeS =50 mg/L, CMC-to-FeS molar ratio = 0.0005, pH =7.0±0.2. Symbols: experimental data; lines: model fittings. Data plotted as mean of duplicates and the error bars (calculated as standard deviation) indicate date reproducibility.

Table 1 Kinetic model parameters

Kinetic model	Parameters	Value
Pseudo-first-order model	q_e (mg g^{-1})	4.907
	k_1 (min^{-1})	28.37
	R^2	0.9978
	RMSE	0.0722
Pseudo-second-order model	q_e (mg g^{-1})	4.943
	k_2 (g mg^{-1} min^{-1})	20.38
	R^2	0.9996
	RMSE	0.0325

3.2 Lead Isotherm

Three models are used to discuss the adsorption isotherm process of Pb(II) onto CMC-FeS, namely the Langmuir [21], the Freundlich [21] and the Sigmoidal models. The equations are shown as below respectively:

Langmuir model: $q_e = \frac{Q_{max} K_L C_e}{1+Q_{max} C_e}$

Freundlich model: $q_e = K_F C_e^{1/n}$

Sigmoidal model: $\frac{q_e}{Q_{max}} = \frac{LC_e}{1+LC_e+\frac{S}{C_e}}$

where q_e (mg g^{-1}) is the adsorption capacity, and C_e (mg g^{-1}) is the concentration of lead at equilibrium. Q_{max} (mg g^{-1}) is the maximum adsorption capacity, and K_L (L mg^{-1}) represents is the Langmuir constant related to the adsorption energy. K_F (mg g^{-1}) is the Freundlich constant related to adsorption capacity, and n is the heterogeneity factor indicating the adsorption intensity of the adsorbate. The Sigmoidal model equation means the S-shape isotherm [23]. The retention of Pb is successfully described by a two-site sigmoidal isotherm equation [24].

The adsorption isotherms are shown in Figure 2, and the corresponding parameters are listed in Table 2. The Figure 2 indicates that the isotherm curve is S-shaped. After curve fitting, we can notice that it can fit sigmoidal model best ($R^2 \approx 0.95$), indicating that the low slope at low concentration is due to formation of strong, nonadsorbing complexes in the solution phase between Pb and CMC. When Pb concentration is higher, the complexing capacity of CMC is exceeded; When CMC competition is lowered, Pb adsorption is enhanced, resulting in the characteristic S-shape isotherm. The FeS surface has a layer of film (CMC) formed, which can increase the adsorption capacity. The synergistic interactions between the adsorption molecules

relates to surface polymerization or surface complexation stereochemical interactions. These interactions result in the sorbate being stable on the sorbent surface, which in turn enhances sorption affinity as the concentration increases. For Sigmoidal model, the maximum sorption capacity is about 77 mg/g at pH 7. For the Bare-particles, the maximum sorption capacity is about 57 mg/g, which is less than CMC-stabilized particles. Whereas, using carbon nanotubes to remove Pb the maximum adsorption capacity is 15.6 mg/g at pH 5 [38]. Using biosorbent, granular AC and powdered AC, the maximum adsorption capacities are 73.7, 15.6 and 26.9 mg/g respectively at pH 5 [39].

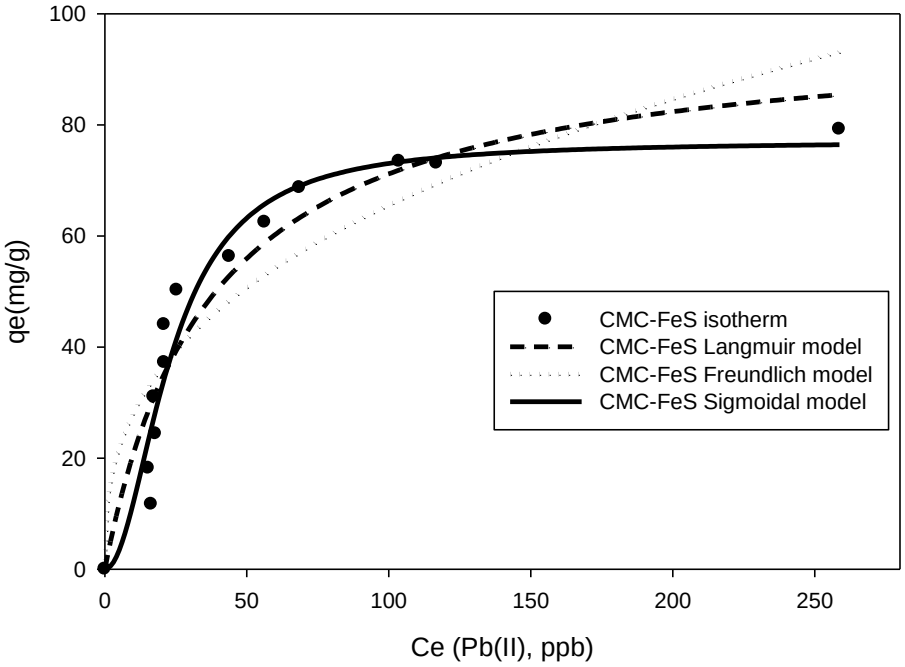

Figure 2. Lead sorption isotherm model fittings of CMC-FeS nanoparticles. FeS = 50 mg/L, CMC-to-FeS molar ratio = 0.0005, initial Pb^{2+} = 500-7000 ppb, pH =7.0±0.2. Symbols: experimental data; lines: model fittings. Data plotted as mean of duplicates and the error bars (calculated as standard deviation) indicate date reproducibility.

Table 2 Isotherm parameters for adsorption of Pb(II) on CMC-FeS

Isotherm	Nonlinear form	Parameters	Value
Langmuir	$q_e = \frac{Q_{max} K_L C_e}{1 + Q_{max} C_e}$	R^2	0.9062
		SEE	8.0651
		Q_{max} (mg g^{-1})	97.7615
		K_L (L mg^{-1})	0.0268
Freundlich	$q_e = K_F C_e^{1/n}$	R^2	0.8171
		SEE	11.2631
		K_F(mg g^{-1})	11.9683
		n	2.7086
Sigmodial	$\frac{q_e}{Q_{max}} = \frac{LC_e}{1 + LC_e + \frac{S}{C_e}}$	R^2	0.9457
		SEE	6.4130
		Q_{max} (mg g^{-1})	77.0364
		L	0.2991
		S	4.5765

3.3 Lead immobilization mechanisms

FTIR spectra of neat CMC, non-stabilized FeS, CMC-FeS, and FeS and CMC-FeS after reaction with Pb (denoted as Pb-laden FeS and Pb-laden CMC-FeS) are depicted in Figure 3. The IR spectra peaks for FeS appear below 400 cm^{-1} [30][32]. For CMC-FeS, four strong peaks are observed at the wave numbers of 3137, 1590, 1412, and 1022 cm^{-1}, respectively, which is ascribed to interactions between COO^- (1590 and 1412 cm^{-1}) or –OH groups (3137 and 1022 cm^{-1}) and Fe^{2+} [22]. Compared with the CMC spectra, the –OH band (3300 cm^{-1}) is shifted to 3137 cm^{-1} for CMC-FeS, which is caused by enhanced intermolecular hydrogen bonding between CMC and FeS surface [22]. The band at 2900 cm^{-1} of neat CMC is shifted to 2923 cm^{-1} of CMC-

FeS, indicating the C-H stretching vibration from the CH_2 groups of the stabilizer [22]. The bands at 1590, 1412, and 1022 cm^{-1} of neat CMC are assigned to asymmetric and symmetric vibrations of COO^- groups and C-O stretching (RCH_2OH) [22]. The wavenumber separation (Δ) between the asymmetric $\nu_{as}(COO^-)$ (1590 cm^{-1}) and symmetric $\nu_s(COO^-)$ (1412 cm^{-1}) stretches is 178 cm^{-1}, suggesting that the primary mechanism for binding CMC to FeS is bidentate bridging [22]. The FTIR spectra of neat CMC, bare FeS, and CMC-FeS suggest that the stabilization of the FeS particles is facilitated through adsorption of CMC molecules onto the surface of the nanoparticles via carboxylate and hydroxyl groups [22]. Thus, CMC stabilizes the nanoparticles through concurrent electrostatic repulsion and steric hindrance [22].

Upon lead sorption, for bare FeS, there are still 2 peaks at 890 and 744 cm^{-1} observed for Pb-laden FeS, which are the absorption proportion of metal-oxygen bond. The entry of Pb^{2+} has entered into but no change the particles crystalline structure [48]. Yet, after reaction with Pb(II), a new weak peak appears at 650 cm^{-1}, which is the IR spectra of PbS precipitation [30]. Compared with CMC-FeS and Pb-laden-CMC-FeS curves, the peak at 880 cm^{-1} of Pb-laden-CMC-FeS curve become weaker but still exists, and a new weak peak is observed at 445 cm^{-1}, which just is a metal-oxygen band like O-Fe [33][34]. The FTIR results indicate that the bare FeS particles take up Pb^{2+} through concurrent chemical precipitation (formation of PbS) and surface complexation, and for CMC-FeS nanoparticles the main reaction is surface complexation.

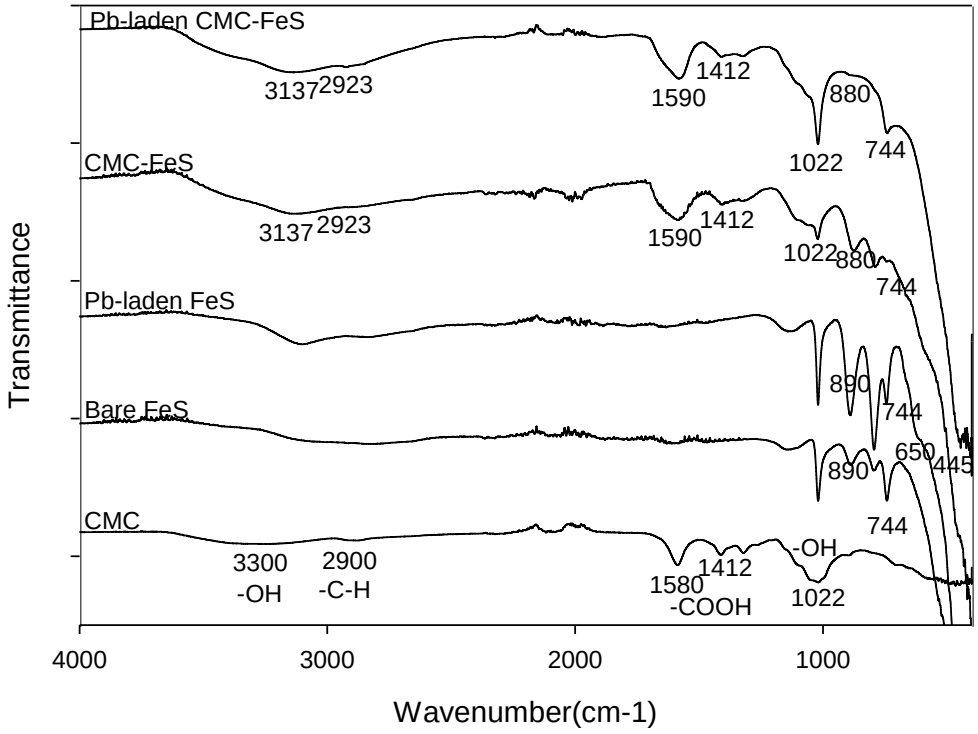

Figure 3. FTIR spectra of neat CMC powder, non-stabilized FeS particles, CMC-FeS nanoparticles, Pb-laden FeS and Pb-laden CMC-FeS. Non-stabilized FeS preparation: FeS = 500 mg/L, and solution pH = 7.0±0.2; CMC-FeS was prepared in the CMC-to-FeS molar ratio 0.0005 under otherwise identical conditions; and Pb-laden FeS was prepared by equilibrating the same non-stabilized FeS with 50 mg/L of Pb^{2+} (several times 250 ppb Pb^{2+} added after equilibrium); and Pb-laden CMC-FeS was prepared by equilibrating the same CMC-FeS with 50 mg/L of Pb^{2+} (several times 250 ppb Pb^{2+} added after equilibrium).

XRD patterns of bare FeS and CMC-FeS before and after lead sorption are compared in Figure 4(a) and 4(b). For bare FeS, the peaks appeared at 2θ values of 36.9°, and 48.9° are indicative peaks of FeS crystals (ICDD, 49-1632) [27][28]. After Pb^{2+} uptake, five new diffraction peaks at 2θ =26.1°, 30.1°, 43.1°, 51.0° and 53.7° are observed corresponding to the characteristic peaks of galena PbS (ICDD, 05-0592, 78-1058) [29]. The diffraction peaks of FeS are still observed after adsorption. The diffraction peaks in Figure 4(b) are disorder, since after stabilized with CMC the CMC-FeS nanoparticles have poor crystallinity. And there are no obvious peaks after Pb adsorption, which indicates that surface complexation is the main reaction during the removal by using CMC-FeS nanoparticles [22]. Moreover, the fact that no PbS is observed may be due to the smaller particle size of CMC-FeS and CMC's inhibitive effect on the growth of crystals [37]. The XRD results support the FTIR results, i.e., CMC-FeS takes up Pb^{2+} mainly through surface complexation.

Based on the XRD and FTIR spectra, the following possible reaction mechanisms for the immobilization of aqueous Pb^{2+} by CMC-FeS are proposed:

(1) Chemical precipitation [22]:

$FeS(s) + H^{+} \Leftrightarrow Fe^{2+} + HS^{-}$

$Pb^{2+} + HS^{-} \Leftrightarrow PbS(s) + H^{+}$

$FeS(s) + Pb^{2+} \Leftrightarrow PbS(s) + Fe^{2+}$

(2) Surface complexation [22]:

$\equiv FeS(s) + Pb^{2+} \Leftrightarrow \equiv FeS - Pb^{2+}$

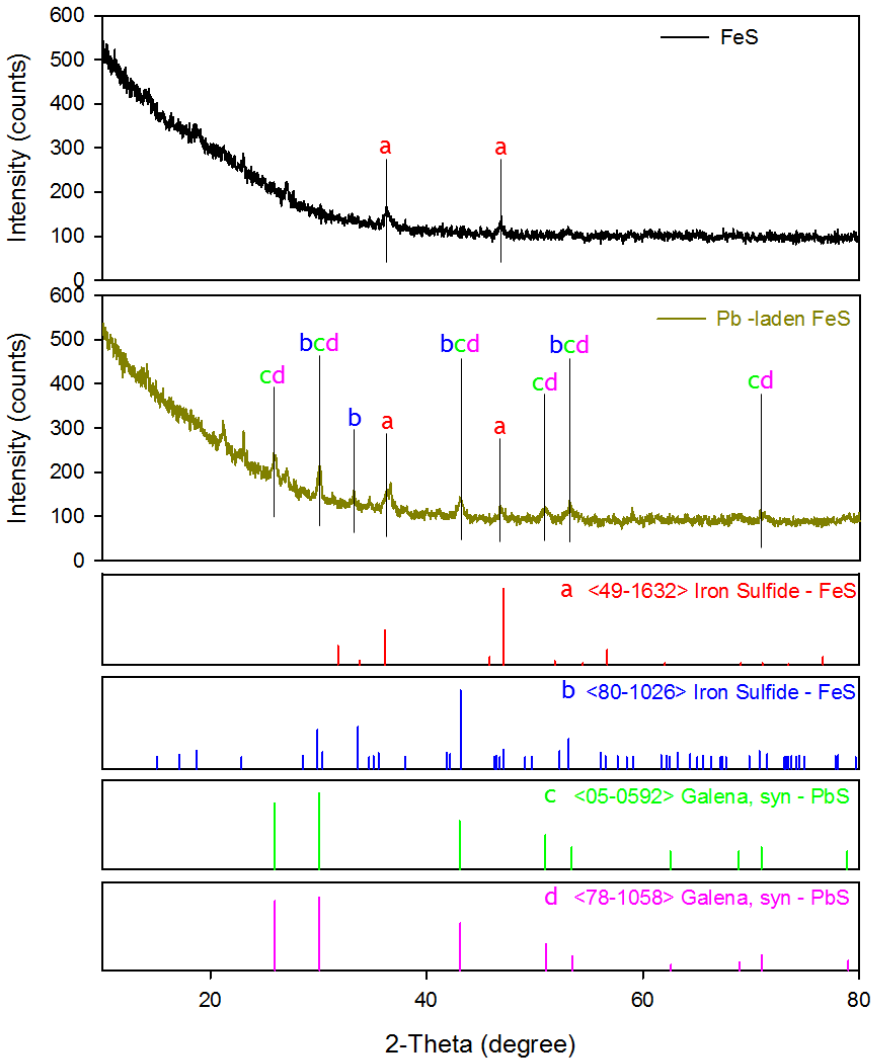

Figure 4(a). XRD spectra of bare FeS nanoparticles, and Pb-laden bare FeS aggregates. Notations: "a" "b" for Iron Sulfide (FeS), "c" "d" for Galena, syn (PbS), XRD powders were prepared in the conditions: FeS = 500 mg/L, Pb^{2+} = 50 mg/L (several times 250 ppb Pb^{2+} added after equilibrium), pH = 7.0±0.2. Bruker D8 Discover X-Ray Diffractometer, Scan 2θ: 10°to 80°, 0.1s/step, 0.01°/step, 6°/min, MDI Jade 6.5, ICDD database.

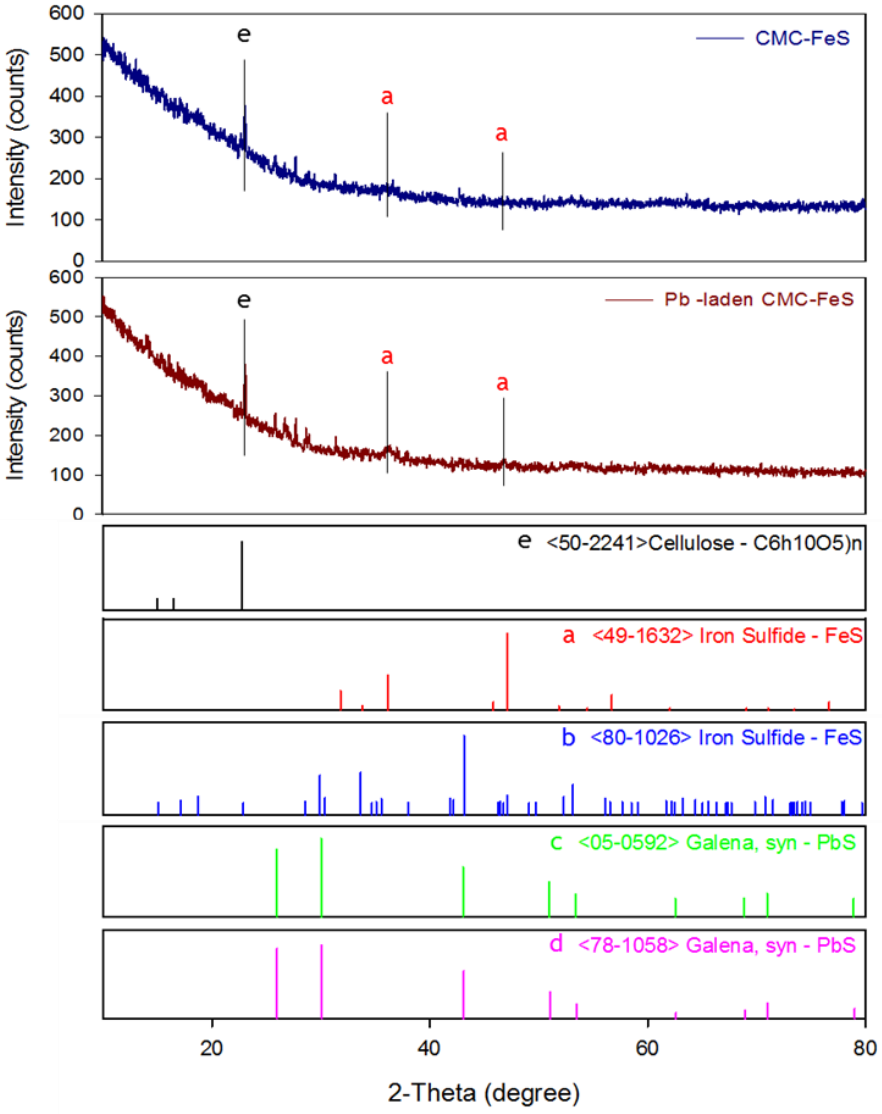

Figure 4(b). XRD spectra of CMC-FeS nanoparticles, and Pb-laden CMC-FeS aggregates. Notations: "a" "b" for Iron Sulfide (FeS), "c" "d" for Galena, syn (PbS), "e" for Cellulose. XRD powders were prepared in the conditions: FeS = 500 mg/L, CMC to FeS ratio 0.0005, Pb^{2+} = 50 mg/L (several times 250 ppb Pb^{2+} added after equilibrium), pH = 7.0±0.2. Bruker D8 Discover X-Ray Diffractometer, Scan 2θ: 10°to 80°, 0.1s/step, 0.01°/step, 6°/min, MDI Jade 6.5, ICDD database.

3.4 Effects of CMC concentration on nanoparticle stability and lead sorption capacity.

FeS particles at a fixed FeS concentration of 50 mg/L but with a variety of CMC concentrations are prepared to determine the CMC effect on the particle stability. After 24 hours of settling by gravity, more than 95% of non-stabilized FeS particles are precipitated. When the CMC concentration increases from 0 to 0.0025 wt % (CMC-to-FeS molar ratio = 0.0005) or higher, the particles remained in the suspension are increased from 15% to 100%. Therefore, a CMC-to-FeS molar ratio of 0.0005 is regarded as the critical stabilization concentration (CSC), defined as the minimum CMC needed to fully stabilize 50 mg/L FeS nanoparticles.

Figure 5 presents the effect of the stabilizer concentration on the equilibrium uptake of Pb^{2+} by FeS particles. Because the initial Pb^{2+} concentration is as low as 250 ppb, there are not obvious large differences for the uptake of Pb^{2+} for different CMC-to-FeS molar ratios. With increasing CMC-to-FeS molar ratio from 0 to 0.0004, Pb^{2+} removal is increased slightly, which can reach a peak uptake at CMC-to-FeS molar ratios of 0.0004-0.0005. Compared to non-stabilized FeS, the stabilized FeS nanoparticles presents 1.5% greater Pb^{2+} uptake. Increasing CMC concentration caused smaller FeS particles, and thus there are greater specific surface area and more sorption sites [22]. However, adding the CMC-FeS ratio above 0.0020 will inhibit Pb^{2+} removal slightly. For example, Pb^{2+} uptake is reduced by 1.5% when the CMC-FeS ratio is increased from 0.0020 to 0.0025. Increasing CMC molecules on the particle surface leads to a denser CMC coating on the nanoparticles, thus limiting the access of Pb^{2+} to the particles' surface sites because of blockage of the sorption sites and/or elevated mass transfer resistance [22]. For the subsequent tests, the optimum CMC-to-FeS molar ratio of 0.0005 is used, considering together both physical stability of the FeS particles and Pb sorption capacity.

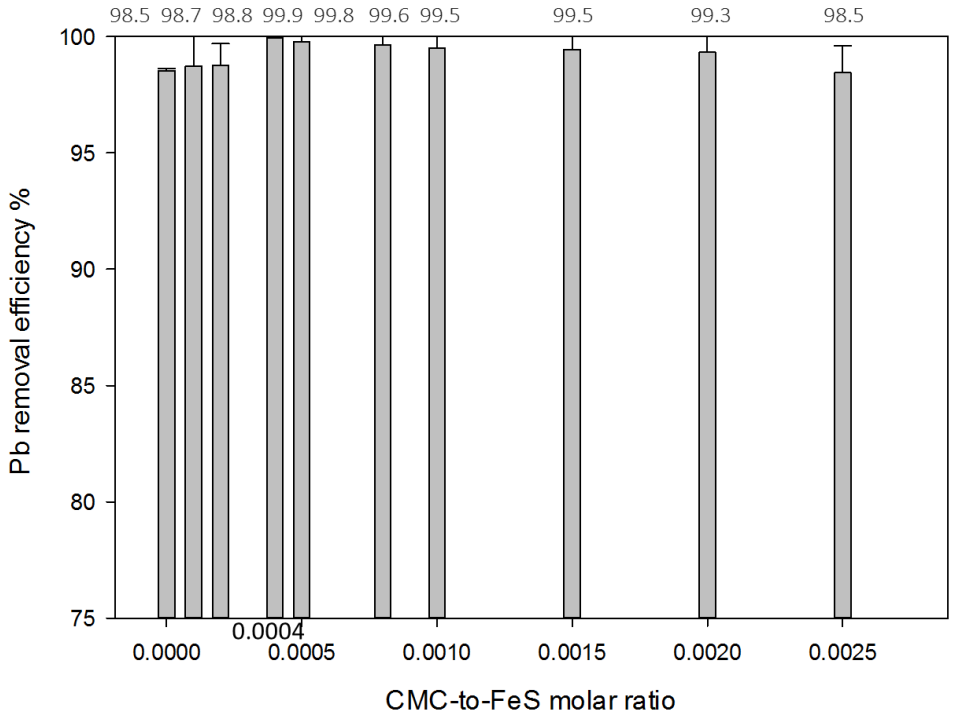

Figure 5. Pb removal efficiency % by FeS nanoparticles prepared at various CMC-to-FeS molar ratios. Initial Pb^{2+} = 250 ppb, FeS =50 mg/L, pH =7.0±0.2. Data plotted as mean of duplicates and the error bars (calculated as standard deviation) indicate date reproducibility.

Figure 6 compares the DLS size of non-stabilized and different CMC-to-FeS molar ratio stabilized FeS particles after modified with measured and calculated viscosity parameters (the specific calculated results shown in Table 3). After 24 hours of settling, the hydrodynamic diameter of the non-stabilized FeS particles is 1073 nm, compared to 50, 333, and 317 nm, respectively, for the completely stabilized particles at a CMC-FeS molar ratio of 0.0005, 0.0010,

and 0.0025. At the CMC-FeS molar ratio of 0.0005, the hydrodynamic diameter of CMC-FeS nanoparticle reaches the smallest value as 50 nm, which supports the CMC effect result that the removal efficiency almost reaches the highest value under this ratio. That is also the reason why the CMC-FeS molar ratio 0.0005 is selected to be used for all experiments in this article.

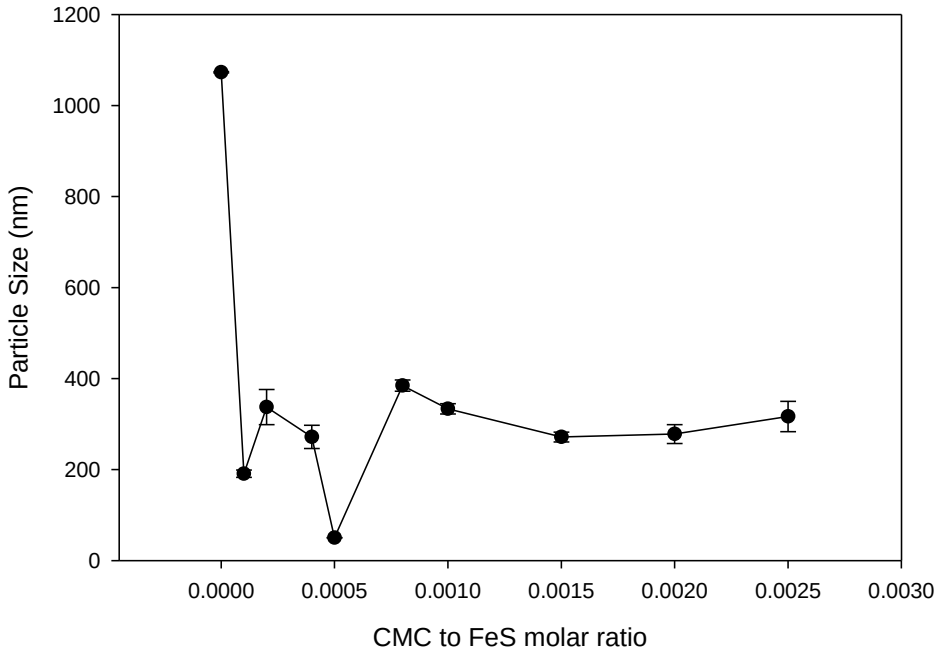

Figure 6. CMC-FeS particle size after modified with viscosity parameter under different CMC to FeS molar ratios. FeS =50 mg/L, CMC-FeS molar ratio = 0.0000 ~ 0.0025, pH =7.0±0.2. Data plotted as mean of duplicates and the error bars (calculated as standard deviation) indicate date reproducibility.

Table 3 Viscosity parameters and calculations

	ρ (CMC+water)	CMC wt%	time(min)		time(ave)	Viscosity μ (cp)
0	1.00000	0.0000%	2.37	2.38	2.38	1.090
1	1.00015	0.0005%	2.55	2.63	2.59	1.189
2	1.00030	0.0010%	2.62	2.62	2.62	1.202
3	1.00060	0.0020%	2.63	2.63	2.63	1.207
4	1.00075	0.0025%	2.56	2.80	2.68	1.230
5	1.00120	0.0040%	2.64	2.69	2.67	1.222
6	1.00150	0.0050%	2.65	2.77	2.71	1.243
7	1.00225	0.0075%	3.20	3.11	3.16	1.446
8	1.00300	0.0100%	3.22	3.21	3.22	1.473
9	1.00375	0.0125%	3.20	3.16	3.18	1.456

Figure 7 shows that the ζ potentials of non-stabilized FeS particle and different CMC-FeS molar ratio particle decrease from -26 mV to -61 mV because of the negative charged CMC. The highly negative surface of CMC-FeS shows that CMC attached on the FeS particles produces strong electrostatic repulsion, which thus avoids the particles from agglomeration. Thus, the CMC stabilizes the nanoparticles through concurrent electrostatic repulsion and steric hindrance [22].

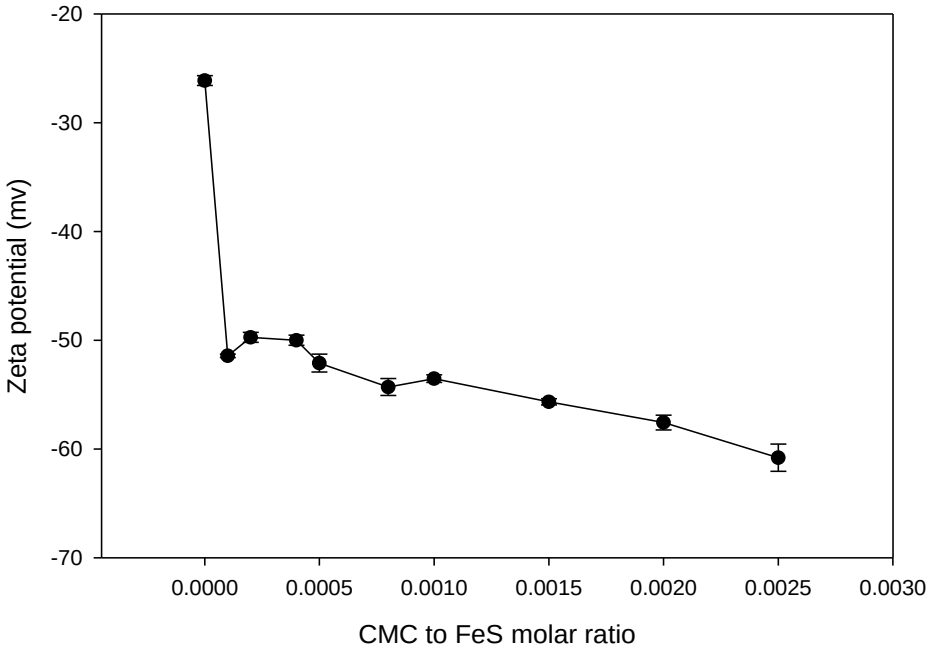

Figure 7. CMC-FeS zeta potential under different CMC to FeS molar ratios. FeS =50 mg/L, CMC-FeS molar ratio = 0.0000 ~ 0.0025, pH =7.0±0.2. Data plotted as mean of duplicates and the error bars (calculated as standard deviation) indicate date reproducibility.

3.5 Effects of CMC-FeS dosage, pH, DOM, and Coexisting ions

Figure 8 shows that increasing the CMC-FeS dosage from 10 to 125 mg/L as FeS results in an increase in the Pb^{2+} removal efficiency from 95% to 99% slightly. The removal efficiency can reach above 90% easily, since the initial Pb^{2+} concentration was low (250 ppb). Further increasing the dosage concentration to 50 mg/L, about 97% of Pb^{2+} is removed. However, the FeS particle is easy to be oxidized during long time filtering, so the FeS dosage of 50 mg/L is selected for all experiments in this article.

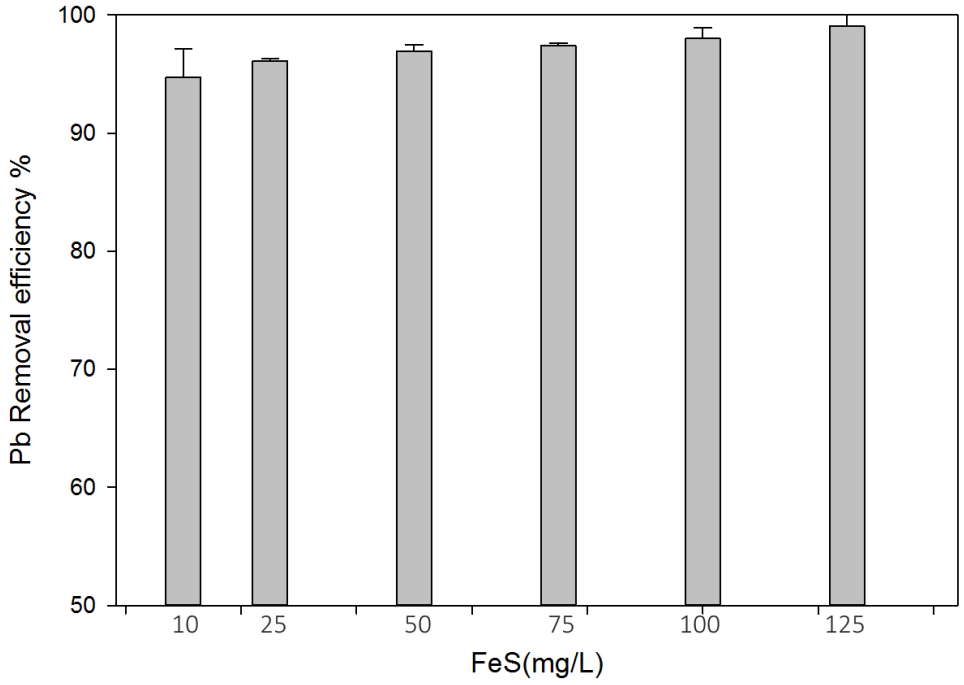

Figure 8. Lead removal efficiency % by various concentrations of FeS with same ratio stabilizer (CMC). Initial Pb^{2+} = 250 ppb, CMC-to-FeS molar ratio = 0.0005, pH =7.0±0.2. Data plotted as mean of duplicates and the error bars (calculated as standard deviation) indicate date reproducibility.

The pH in solution affects the percentage of FeS particles and the concentration of metal species, and thus pH is a significant factor in adsorption. Figure 9 shows the effect of pH and FeS leaching on adsorption of Pb(II) by CMC-FeS. The x-axis is the final pH after equilibrium. For the initial pH 4.0, 4.5, 5.0, 5.5, 6.0 and 6.5, the final pH increase to 4.5, 6.0, 6.1, 6.1, 6.2 and 6.6, respectively. The CMC-FeS pH is about 7.0 after aged 24 hours, thus after add HCl to adjust the pH to lower, the pH tends to rebound. But for the initial pH 7.0, the final pH decreases to 6.9 slightly. Since the solubility product constant of $Pb(OH)_2$ is low (Ksp (25°C) = 1.43×10^{-20}),

when pH < 7, $PbCl_2$ is dissolved in water to produce Pb^{2+} and $Pb(OH)^+$ slightly [25], and the main hydrolysis reaction shows as below. At pH 7, mainly 70% Pb^{2+} exist in the lead solution [25]. During the removal, precipitation and surface complexation consume Pb^{2+} or $Pb(OH)^+$, which causes the hydrolysis reaction going to right side to produce more H^+ and to make the final pH decrease slightly during the whole experiments in this article at initial pH 7.

$$2PbCl_2 + H_2O \rightleftharpoons Pb^{2+} + Pb(OH)^+ + H^+ + 4Cl^-$$

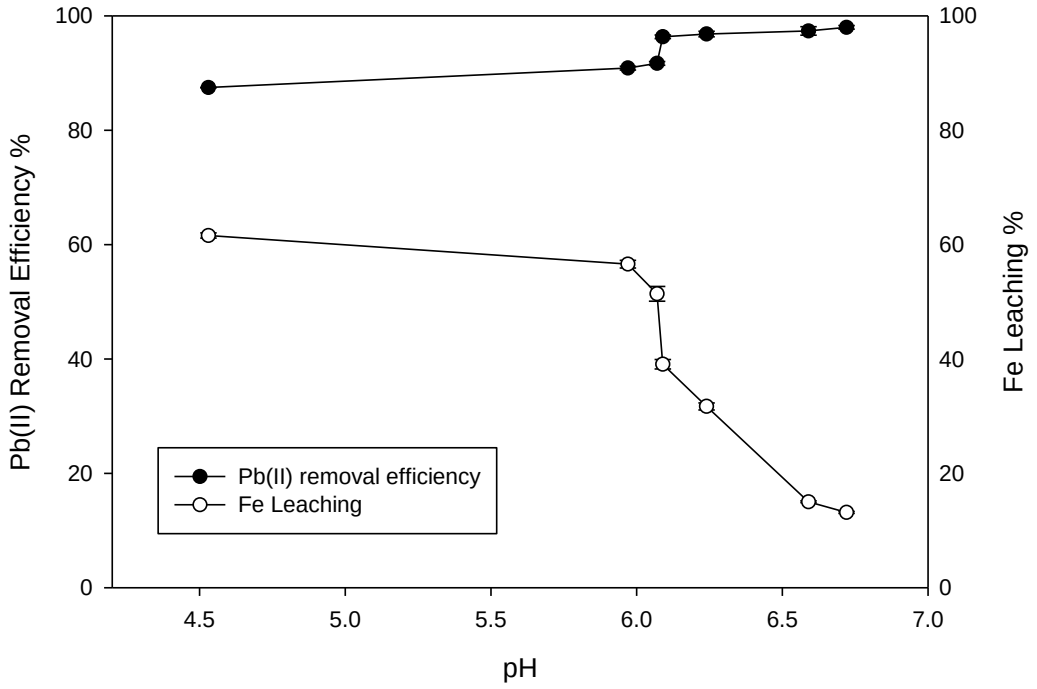

Figure 9. Effect of equilibrium pH on lead removal efficiency % and Fe leaching % by CMC-FeS. FeS =50 mg/L, CMC-to-FeS molar ratio = 0.0005, initial Pb^{2+} = 250 ppb, initial pH are 4.0, 4.5, 5.0, 5.5, 6.0, 6.5, 7.0. Data plotted as mean of duplicates and the error bars (calculated as standard deviation) indicate date reproducibility.

With the increase of pH, the adsorption capacities of lead species arise, because at low pH the particle FeS leaches more than 50%. At pH range from 6.5 to 7, the removal efficiencies are more than 95%, and at this range, the Fe leaching is about 15%. Lower pH dissolves FeS, which is good for the chemical precipitation, and bad for surface complexation. Combined with XRD results, for CMC-FeS nanoparticles the function of surface complexation is larger than the precipitation. Therefore, for removal lead by using CMC-FeS nanoparticles, the optimal pH range is 6.5~7.0.

Figure 10 shows that the removal efficiency decreases slightly with Humic Acid concentration increasing from 0 ppm to 10 ppm as TOC. After curve fitting, the Figure 11 illustrates that the kinetic results are closely fitted by the pseudo-second-order model, which is same as the general kinetic test in 3.1 part. Table 4 shows the specific parameters k_2 increase with the HA concentration increasing. Based on pseudo-second-order model equation, the larger k_2 value the slower the adsorption rate [26]. Therefore, humic acid has a slight inhibiting effect for Pb^{2+} removal. The first reason is that, for complexing with the aqueous lead, DOM can compete with FeS. For example, two-coordinate complexes with organic thiol groups of DOM are formed with Pb^{2+}. Then, DOM can compete with CMC molecules for sites on FeS nanoparticles, changing the stabilizing effectiveness of CMC, the ζ potential, and thus, aggregation of the nanoparticles.

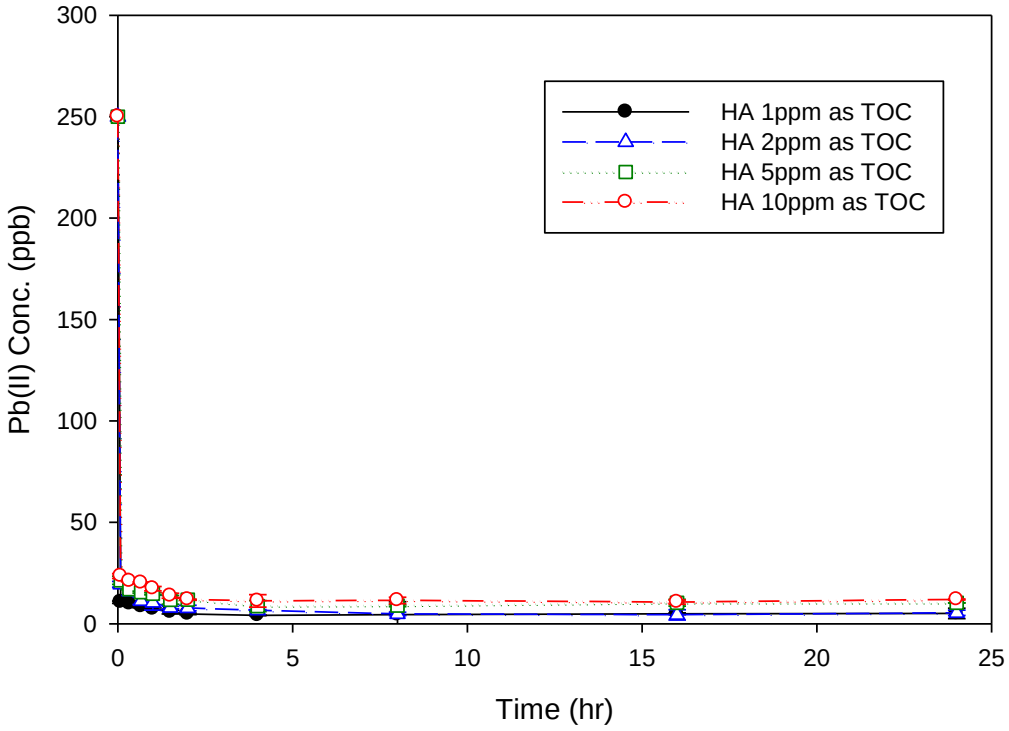

Figure 10. Effect of HA on lead uptake by CMC-FeS. FeS =50 mg/L, CMC-to-FeS molar ratio = 0.0005, initial Pb^{2+} = 250 ppb, pH =7.0±0.2. Data plotted as mean of duplicates and the error bars (calculated as standard deviation) indicate date reproducibility.

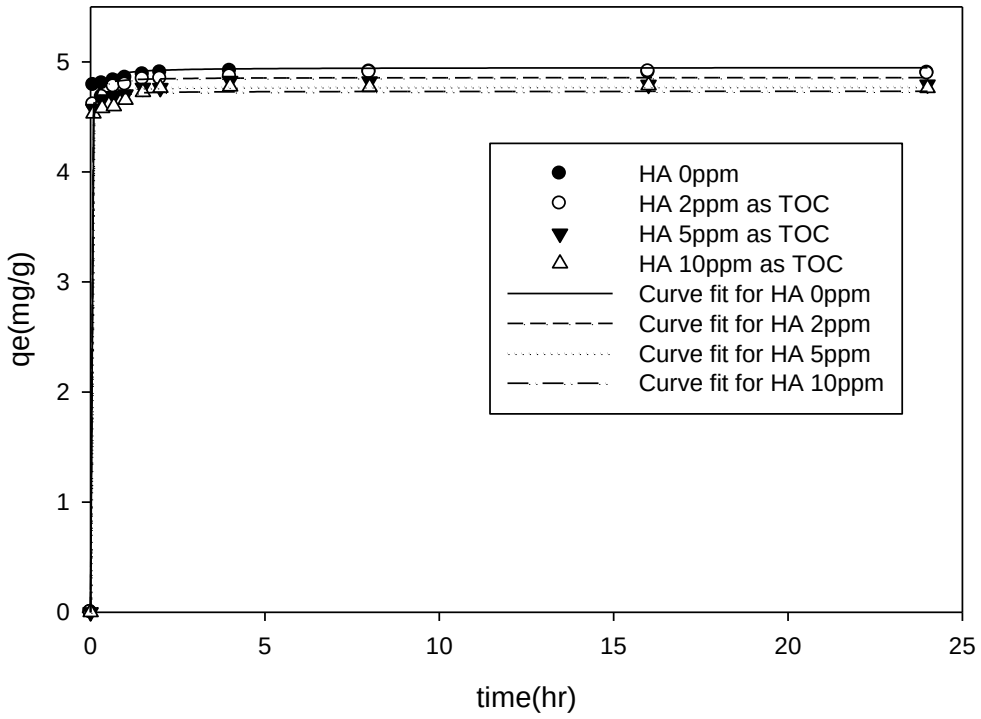

Figure 11. Effect of HA Pseudo-second-order kinetic fittings of lead sorption by CMC-FeS. Initial Pb^{2+} = 250 ppb, FeS =50 mg/L, CMC-to-FeS molar ratio = 0.0005, pH =7.0±0.2. Symbols: experimental data; lines: model fittings. Data plotted as mean of duplicates and the error bars (calculated as standard deviation) indicate date reproducibility.

Table 4 HA as TOC effects Kinetic model (Pseudo-second-order model) parameters

HA as TOC	k_2	Ce
0ppm	20.38	1.5561
2ppm	39.78	5.3769
5ppm	49.67	10.2902
10ppm	46.70	11.9875

Figure 12 (a) and (b) present the effects of coexisting Na^+ and Ca^{2+} ions on adsorption of lead, respectively. The adsorption capacity of Pb(II) decreases with increasing inorganic ion concentration, since the coexisting cations compete for adsorption sites with Pb(II). Bivalent Ca^{2+} has a larger affinity with CMC-FeS than Na^+, so the inhibition effect becomes more obvious.

(a)

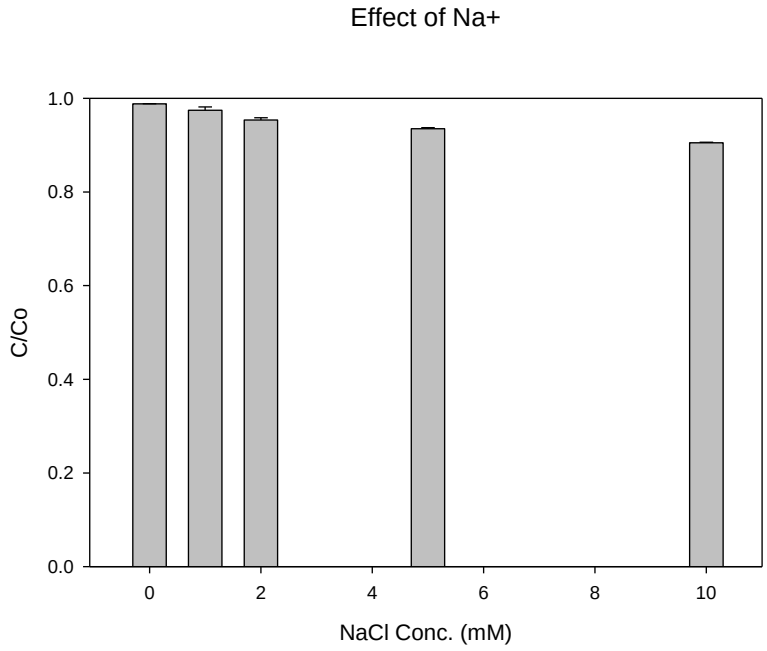

(b)

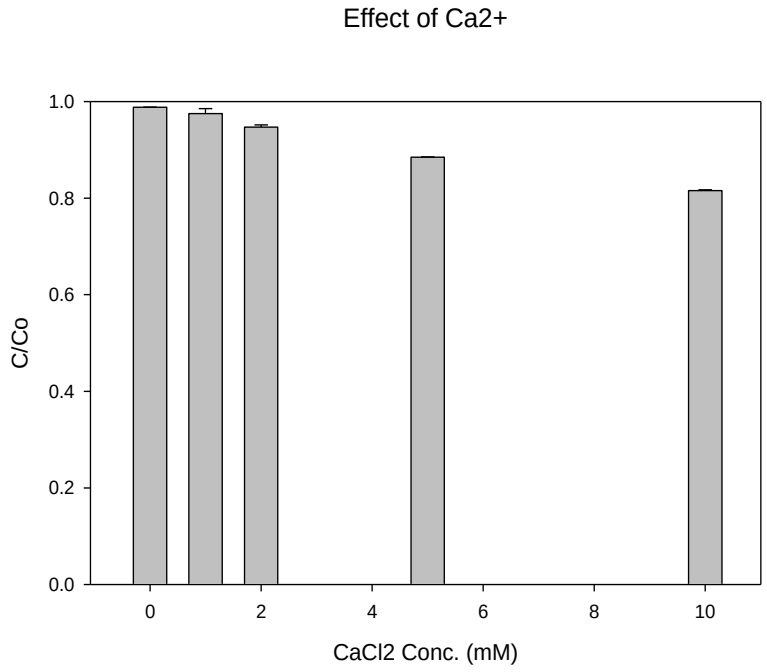

Figure 12. Effects of coexisting ion (a) Na^+ and (b) Ca^{2+} on sorption of lead by CMC-FeS.

Initial Pb^{2+} = 250 ppb, FeS =50 mg/L, CMC-to-FeS molar ratio = 0.0005, pH=7.0±0.2.

Chapter 4

Conclusions and Recommendations for Future Work

4.1 Conclusions

This study investigated the effectiveness of CMC-FeS nanoparticles for removing lead in aqueous phase. The main findings are summarized as follows:

(1) The sorption kinetics of Pb(II) is very rapid, which can fit the Pseudo-second-order model, and the rate-controlling step for the sorption is chemical interaction.

(2) The sorption isotherm of Pb(II) fits closely to the Sigmoidal model with a calculated maximum sorption capacity of 77 mg g^{-1}. The sorption isotherm of Pb(II) presents the S-shape, which indicates that in the beginning the nonadsorbing complexes in the solution phase between Pb and CMC form, when Pb concentration is higher, the complexing capacity of CMC is exceeded. When CMC competition becomes lowered, Pb sorption is enhanced. Namely, these interactions cause the sorbate to be stabilized on the sorbent surface, which in turn enhances sorption affinity as the Pb concentration goes up.

(3) FTIR and XRD analyses further confirm the mechanism that both precipitation (formation of galena) and surface complexation are the main reactions during the lead removal. CMC molecules attach to the nanoparticles through bidentate bridging and hydrogen bonding.

(4) The optimum CMC-FeS concentration is 0.0025 wt% - 50 mg/L (CMC-to-FeS molar ratio is 0.0005) in this research. Under this condition, the DLS size of CMC-FeS nanoparticles is 50 nm, and the zeta potential is about -53 mV.

(5) Laboratory tests reported herein show that the sorption capacities of Pb(II) can be increased with increasing pH from 4 to 7. But in pH range of 6.5~7.0, the leachability of FeS particle is

the lowest. Thus, the optimum pH for lead uptake by using CMC-FeS is approximately 6.5~7.0.

(6) Humic acid has a slight inhibiting effect for Pb^{2+} removal with the same kinetic pseudo-second-order model curve fitting. Co-existing Na^{+} and Ca^{2+} slightly decreases the sorption capacity of Pb(II), indicating that CMC-FeS has good sorption selectivity for existing ions.

4.2 Recommendations for Future Work

Besides some other heavy metals, radionuclides, chlorinated organic compounds, nitroaromatic compounds, and polychlorinated biphenyls, the CMC-FeS nanoparticles can remove the heavy metal pollutant Pb(II) efficiently. And CMC-FeS has the potential for treat the wastewater includes many kinds of pollutants. CMC-FeS can be used to immobilize pollutants in site, thus, the research about CMC-FeS remove Pb(II) in field soil and sediment should be continued in the future.

References

[1] Abadin H, Ashizawa A, Stevens YW, et al. Agency for Toxic Substances and Disease Registry (ATSDR) Toxicological Profiles. Toxicological Profile for Lead. Atlanta (GA): U.S. DEPARTMENT OF HEALTH AND HUMAN SERVICES. 2007.

[2] Bremner, H. A. (2002). Safety and Quality Issues in Fish Processing. Elsevier. ISBN 978-1-85573-678-8.

[3] Agency for Toxic Substances and Disease Registry. "Information for the Community: Lead Toxicity" (MP4 webcast, 82 MB). Retrieved 11 February 2017.

[4] Song, Q., Li, J., 2014. Environmental effects of heavy metals derived from the e-waste recycling activities in China: a systematic review. Waste Manag. 34, 2587–2594. http://dx.doi.org/10.1016/j.wasman.2014.08.012.

[5] Tang, R.L., Ma, K.M., Zhang, Y.X., Mao, Q.Z., 2013. The spatial characteristics and pollution levels of metals in urban street dust of Beijing, China. Appl. Geochem. 35, 88–98.

[6] Li, Z.G., Feng, X.B., Li, G.H., Bi, X.Y., Zhu, J.M., Qin, H.B., et al., 2013c. Distributions, sources and pollution status of 17 trace metal/metalloids in the road dust of a heavily industrialized city of central China. Environ. Pollut. 182, 408–416.

[7] Wang HY, Lu SG. Spatial distribution, source identification and affecting factors of heavy metals contamination in urban–suburban soils of Lishui city. China Environ Earth Sci 2011; 64:1921–9

[8] Yuan GL, Sun TH, Han P, Li J, Lang XX. Source identification and ecological risk assessment of heavy metals in topsoil using environmental geochemical mapping: typical

urban renewal area in Beijing, China. J Geochem Explor 2014;136:40–7.

[9] Speak AF, Rothwell JJ, Lindley SJ, Smith CL. Metal and nutrient dynamics on an aged intensive green roof. Environ Pollut 2014;184:33–43.

[10] Gunawardena, J., Egodawatta, P., Ayoko, G.A., Goonetilleke, A., 2013. Atmospheric deposition as a source of heavy metals in urban stormwater. Atmos. Environ. 68, 235e242.

[11] F.L. Fu, Q. Wang, Removal of heavy metal ions from wastewaters: a review, J. Environ. Manage. 92 (2011) 407–418.

[12] Wu, G., Kang, H., Zhang, X., Shao, H., Chu, L., Ruan, C., 2010. A critical review on the bio-removal of hazardous heavy metals from contaminated soils: issues, progress, eco-environmental concerns and opportunities. J. Hazard. Mater. 174, 1–8

[13] Ayangbenro, A. S. and Babalola, O. O. (2017): A New Strategy for Heavy Metal Polluted Environments: A Review of Microbial Biosorbents. Int. J. Environ. Res. Public Health, 14 (94): 1-16. DOI: 10.3390/ijerph14010094

[14] Y. Gong, J. Tang, D. Zhao, Application of iron sulfide particles for groundwater and soil remediation: a review, Water Res. 89 (2016) 309–320, http://dx.doi. org/10.1016/j.watres.2015.11.063.

[15] Zhao D, Xiong Z, Barnett M, Liu R, Harper WF, He F (2009) In situ immobilization of metals in contaminated sites using stabilized iron phosphate nanoparticles. US Patent 7581902B2

[16] Zhao D, He F. (Auburn, AL, US). Preparation and applications of stabilized metal nanoparticles for dechlorination of chlorinated hydrocarbons in soils, sediments, and ground water; 2008. United States.

[17] Özverdi A, ErdemM. Cu^{2+}, Cd^{2+} and Pb^{2+} adsorption from aqueous solutions by pyrite and synthetic iron sulphide. J Hazard Mater. 2006;137(1):626–32.

[18] Ito D, Miura K, Ichimura T, Ihara I, Watanabe T. Removal of As, Cd, Hg and Pb ions from solution by adsorption with bacterially produced magnetic iron sulfide particles using high gradient magnetic separation. IEEE T Appl Supercon. 2004;14(2):1551–3.

[19] Watson, J.H.P., Ellwood, D.C., Deng, Q., Mikhalovsky, S., Hayter, C.E., Evans, J., 1995. Heavy metal adsorption on bacterially produced FeS. Miner. Eng. 8 (10), 1097e1108.

[20] Xiong Z, He F, Zhao D, et al. Immobilization of mercury in sediment by stabilized iron sulfide (FeS) nanoparticles. Water Res, 2009, 43: 5171

[21] W. Liu, P. Zhang, A.G.L. Borthwick, H. Chen, J. Ni, Adsorption mechanisms of thallium(I) and thallium(III) by titanate nanotubes: ion-exchange and coprecipitation, J. Colloid Interface Sci. 423 (2014) 67–75.

[22] Y. Gong, Y. Liu, Z. Xiong, D. Zhao, Immobilization of mercury by carboxymethyl cellulose stabilized iron sulfide nanoparticles: reaction mechanisms and effects of stabilizer and water chemistry, Environ. Sci. Technol. 48 (2014) 3986–3994.

[23] G. Limousin, J.-P. Gaudet, L. Charlet, S. Szenknect, V. Barthe's, M. Krimissa, Sorption isotherms: a review on physical bases, modeling and measurement, Appl. Geochem. 22 (2007) 249–275.

[24] Selim, H.M., Amacher, M.C., 1996. Reactivity and Transport of Heavy Metals in Soils. CRC Press, Boca Raton, FL.

[25] Yang, S.T., Zhao, D.L., Zhang, H., Lu, S.S., Chen, L., Yu, X.J., 2010. Impact of environmental conditions on the sorption behavior of Pb(II) in Na-bentonite suspensions.

J. Hazard. Mater. 183, 632e640.

[26] M.-E. Lee, J.H. Park, J.W. Chung, C.-Y. Lee, S. Kang, Removal of Pb and Cu ions from aqueous solution by Mn3O4-coated activated carbon, J. Ind. Eng. Chem. 21 (2015) 470–475.

[27] Yue Sun, Dan Lv, J. Zhou, X. Zhou, Z. Lou, S.A. Baig, X. Xu, Adsorption of mercury (II) from aqueous solutions using FeS and pyrite: A comparative study, Chemosphere, Vol.185, (2017) 452-461.

[28] L.H. Zhou, X.C. Wei, Z.J. Ma, B. Mei, Anti-friction performance of FeS nanoparticles synthesized by biological method, Applied Surface Science, Vol.407, (2017) 21-28.

[29] N.M. Huang, S. Radiman, H.N. Lim, S.K. Yeong, P.S. Khiew, W.S. Chiu, S.N. Kong, G.H. Mohanmed Saeed, Synthesis and characterization of ultra small PbS nanorods in sucrose ester microemulsion, Materials Letters, 63 (2009), pp. 500-503.

[30] M. Salavati-Niasari, A. Sobhani, F. Davar, Synthesis of star-shaped PbS nanocrystals using single-source precursor, J. Alloys Compd., 507 (2010), p. 77

[31] Lauterbach, L.et al.Nuclear resonance vibrational spectroscopy reveals the FeScluster composition and active site vibrational properties of an O2-tolerantNAD(þ)-reducing [NiFe] hydrogenase.Chem. Sci.6,1055–1060 (2015)

[32] R.C. Chikate, S.B. Padhye, Transition metal quinone–thiosemicarbazone complexes 2: magnetism, ESR and redox behavior of iron (II), iron (III), cobalt (II) and copper(II) complexes of 2-thiosemicarbazido-1, 4-naphthoquinone, Polyhedron 24 (2005) 1689–1700

[33] M. Aydın, B. U¨ nal, B. Esat, A. Baykal, E. Karaoglu, M.S. Toprak, H. So¨zeri, J.

Alloys Compd. 514 (2012) 45–53.

[34] A. Azam, A. Jawad, A.S. Ahmed, M. Chaman, A.H. Naqvi, J. Alloys Compd. 509 (2011) 2909–2913.

[35] Flora, G., Gupta, D., Tiwari, A., 2012. Toxicity of lead: a review with recent updates. Interdiscip. Toxicol. 5, 47e58.

[36] Rahman L, Islam M, Hossain MZ, Ahsan MA (2012). Study of the seasonal variations in Turag River water quality parameters. Afr. J. Pure Appl. Chem. 6(10):144-148.

[37] Gong, Y.; Liu, Y.; Xiong, Z.; Kaback, D.; Zhao, D. Immobilization of mercury in field soil and sediment using carboxymethyl cellulose stabilized iron sulfide nanoparticles. Nanotechnology 2012, 23 (29), 294007.

[38] Li YH,Wang S,Wei J, Zhang X, Xu C, Luan Z,Wu D,Wei B. Lead adsorption on carbon nanotubes. Chem Phys Lett 2002; 357:263–6.

[39] Z. Reddad, C. G´erente, Y. Andres, P. Le Cloirec, Adsorption of several metal ions onto a low-cost biosorbent: kinetic and equilibrium studies, Environ. Sci. Technol. 36 (2002) 2067–2073.

[40] Pain, D.J., 1996. Lead in waterfowl. In: Beyer, W.M., Heinz, G.H., Redman-Norwood, A.W. (Eds.), Environmental Contaminants in Wildlife: Interpreting Tissue Concentrations. Lewis Publishers, Boca Raton, pp. 251–262.

[41] Rudolph, A. M.; Rudolph, C. D.; Hostetter, M. K.; et al. (2003). "Lead". Rudolph's Pediatrics (21st ed.). McGraw-Hill Professional. p. 369. ISBN 978-0-8385-8285-5.

[42] Dart, R. C.; Hurlbut, K. M.; Boyer-Hassen, L. V. (2004). "Lead". In Dart, R. C.

Medical Toxicology (3rd ed.). Lippincott Williams & Wilkins. p. 1426. ISBN 978-0-7817-2845-4.

[43] Tong S, von Schirnding YE, Prapamontol T. Environmental lead exposure: a public health problem of global dimensions. [Review]. Bull World Health Organ 2000; 78: 1068–77.

[44] Mushak P. Defining lead as the premier environmental health issue for children in America: criteria and their quantitative application. Environmental Research, 1992, 59: 281–309.

[45] Tong S, McMichael AJ. The magnitude, persistence and public health significance of cognitive effects of environmental lead exposure in childhood. Journal of Environmental Medicine, 1999, 1: 103–110.

[46] Schwartz J. Low level lead exposure and children's IQ: a meta analysis and search for a threshold. Environmental Research, 1994, 65: 42–55.

[47] Ruff HA et al. Declining blood lead levels and cognitive changes in moderately lead-poisoned children. Journal of the American Medical Association, 1993, 269: 1641–1646.

[48] Bing P, Xiujun L, Shuangheng M, Bin, W. Modifying Mg/Al Composite Catalyst for Preparing Narrow-range Distribution Polyether, Modern Applied Science, ISSN 1913-1844, 2007, Vol. 1, No. 3.

Appendices

Supporting Information

Detection Limit of Pb

During the research, main data is measured by using ICP-OES 710-ES. In order to make the data's reasonability, it is necessary to obtain the Detection Limit of Pb for this research. Besides Figure 16 shows the official Detection Limit of the ICP-OES 710-ES from the Agilent Technologies Company, which presents that the Detection Limit of Pb is 1.0 ppb. Figure 17 shows the main procedure to prepare the different lead solutions with different lead concentrations (0, 1 ppb, 2 ppb, 5 ppb and 10 ppb) by different preparation flows. And we measure the Pb concentration of the solutions three times by ICP-OES 710-ES continually.

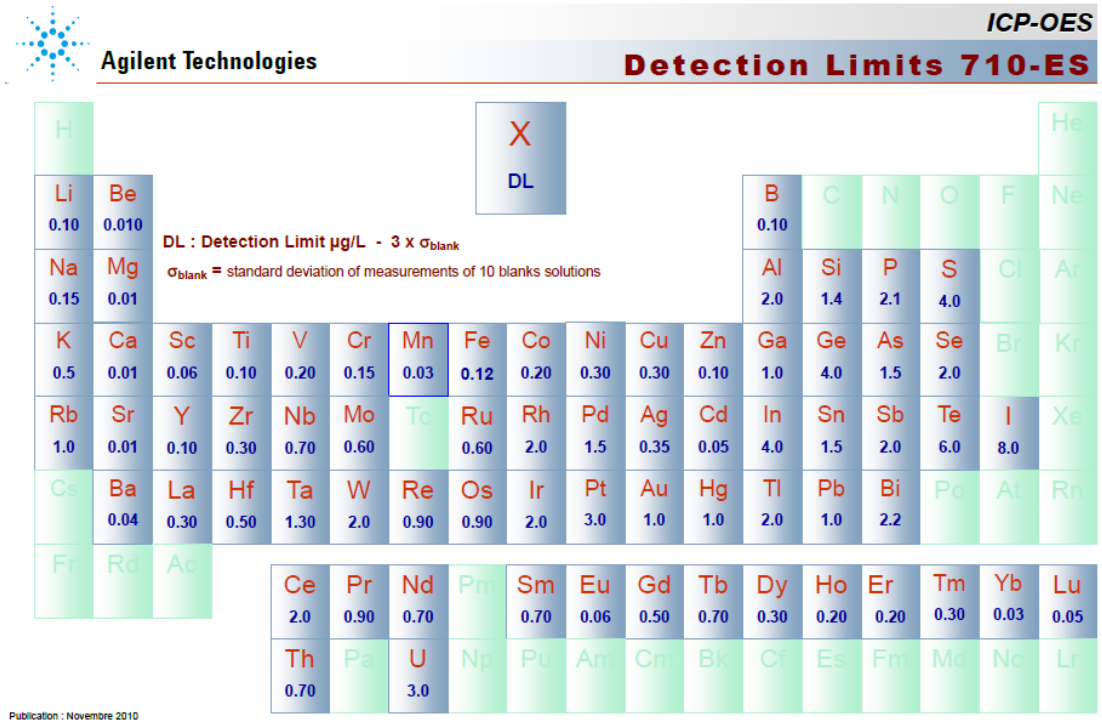

Figure 13. ICP-OES 710-ES Detection limits data from Agilent Technologies Company

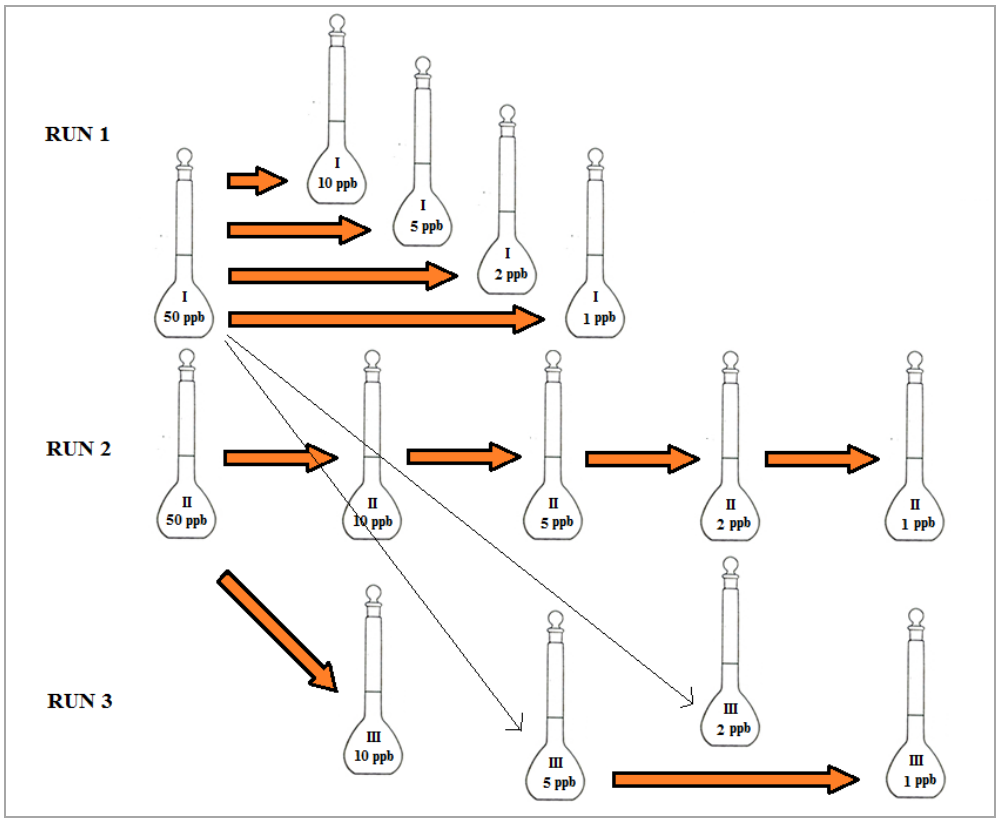

Figure 14. Pb solutions preparation for Detection Limit

Table 5 shows the results for Detection Limit of Pb. From the average values, the concentration of Pb 5 ppb can be detected steadily. Therefore, for the research the Detection Limit of Pb is 5 ppb. In the experiments, if the Pb concentration obtained by ICP-OES is below 5 ppb, the concentration is modified into 5 ppb automatically for data analysis.

Table 5 Detection Limit for the experiment

	10 ppb	5 ppb	2 ppb	1 ppb	DI water
I	9.17	5.55	1.40	0.77	-4.53
	9.46	3.37	2.85	1.87	1.34
	8.26	4.33	-0.08	1.45	-0.18
Ave.	8.96	4.42	1.39	1.36	-1.12
II	8.61	5.15	-0.15	-1.18	-0.34
	8.86	4.00	1.02	1.40	-2.56
	8.60	4.21	-0.50	0.74	-2.87
Ave.	8.69	4.45	0.12	0.32	-1.92
III	9.09	4.30	1.45	2.51	0.61
	12.10	5.36	4.09	1.14	-1.01
	11.13	5.12	2.38	3.29	-0.42
Ave.	10.77	4.93	2.64	2.31	-0.27
Total Ave.	9.47	4.60	1.38	1.33	-1.11

The impact of the Nitrocellulose Membrane on Pb concentration

In order to check whether the filter membrane we used during the whole experiment influences the Pb concentration, we also did the related experiments to measure the concentration difference between Pb solutions before and after filtered by using the Nitrocellulose Membrane. After measurements, the results show that the Pb concentration decreases about 2% after filtered with

the membrane, and the Pb solution mixed with same amount of CMC (0.0025 wt %) keeps the same concentration after filtered with the membrane.

Lead species distribution as a function of pH

Lead species are easy to precipitate in solution based on the low K_{sp} of $Pb(OH)_2$. Therefore, the lead species distribution as a function of pH is discussed and shown in this part for supporting the main mechanism for the immobilization of lead by carboxymethyl cellulose stabilized iron sulfide nanoparticles.

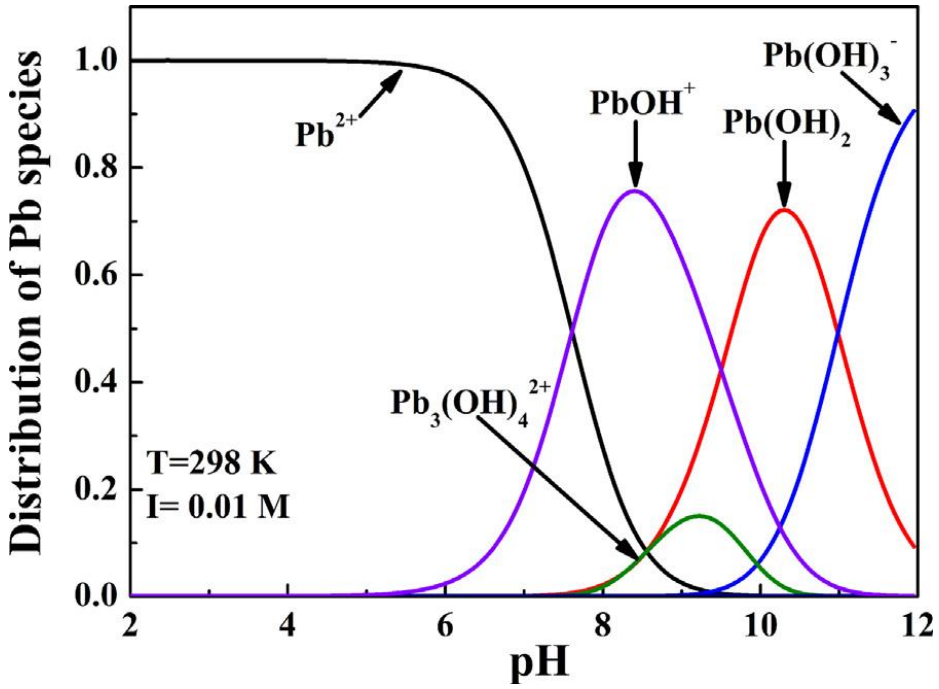

Figure 15. Distribution of Pb species as a function of pH [25]

Figure 18 shows the distribution of lead species at different pH. It is known that lead species present in the forms of Pb^{2+}, $Pb(OH)^{+}$, $Pb(OH)_2^{0}$, $Pb(OH)^{3-}$at different pH values. As for Pb^{2+} ion, the existing form of Pb^{2+} will also change under different pH values. Therefore, the ion form

Pb^{2+} mainly exists in the first region (pH = 2–7), while at pH 7 mainly 70% lead specie exists in in the form of Pb^{2+} [25].